ARL-TR-9557 ● SEP 2022

DEVCOM ARMY RESEARCH LABORATORY

Cold Sintering of Zinc Oxide (ZnO) and Silica (SiO_2)

by Andrew Rosenberger, Victoria Blair, Leah Hlubb, and Michael Golt

NOTICES

Disclaimers

The findings in this report are not to be construed as an official Department of the Army position unless so designated by other authorized documents.

Citation of manufacturer's or trade names does not constitute an official endorsement or approval of the use thereof.

Destroy this report when it is no longer needed. Do not return it to the originator.

ARL-TR-9557 ● SEP 2022

Cold Sintering of Zinc Oxide (ZnO) and Silica (SiO_2)

Victoria Blair and Michael Golt
DEVCOM Army Research Laboratory

Andrew Rosenberger
Bennett Aerospace

Leah Hlubb
College Qualified Leaders Program, Rochester Institute of Technology

REPORT DOCUMENTATION PAGE

Form Approved
OMB No. 0704-0188

1. REPORT DATE *(DD-MM-YYYY)*	2. REPORT TYPE	3. DATES COVERED (From - To)
September 2022	Technical Report	October 2019–June 2022

4. TITLE AND SUBTITLE
Cold Sintering of Zinc Oxide (ZnO) and Silica (SiO_2)

5a. CONTRACT NUMBER

5b. GRANT NUMBER

5c. PROGRAM ELEMENT NUMBER

6. AUTHOR(S)
Andrew Rosenberger, Victoria Blair, Leah Hlubb, and Michael Golt

5d. PROJECT NUMBER

5e. TASK NUMBER

5f. WORK UNIT NUMBER

7. PERFORMING ORGANIZATION NAME(S) AND ADDRESS(ES)
DEVCOM Army Research Laboratory
ATTN: FCDD-RLW-ME
Aberdeen Proving Ground, MD 21005

8. PERFORMING ORGANIZATION REPORT NUMBER
ARL-TR-9557

9. SPONSORING/MONITORING AGENCY NAME(S) AND ADDRESS(ES)

10. SPONSOR/MONITOR'S ACRONYM(S)

11. SPONSOR/MONITOR'S REPORT NUMBER(S)

12. DISTRIBUTION/AVAILABILITY STATEMENT
Approved for public release: distribution unlimited.

13. SUPPLEMENTARY NOTES
ORCID IDs: Andrew Rosenberger, 0000-0003-3993-4866; Victoria Blair, 0000-0003-1340-7144; Michael Golt, 0000-0003-4685-0695

14. ABSTRACT
Cold sintering was investigated as a potential densification method for silica polymorphs. Initial experiments achieved a porosity of 5.1% when using amorphous silica powder in 25 wt% of 5-M sodium hydroxide (NaOH) solution at 250 °C and 500 MPa for 24 h. A design of experiments study investigated the influence of pressure, silica phase, timing of the heating relative to load, and NaOH concentration on densification. Higher NaOH concentrations and applying pressure before heating helped maximize density. A two-way interaction between either NaOH concentration and powder phase or pressure and heating timing was also identified. The dependence on silica phase and chemistry were explored by comparing the cold sintering of neat and metal ion doped amorphous silica and the cristobalite and quartz phases of silica under the same conditions. Cold sintered amorphous silica had a final mean porosity of 8.0 ±2.7%, compared to quartz's 19.1% and cristobalite's 12.5%. X-ray diffraction determined that all sintered specimens comprised primarily of quartz, but cristobalite could be retained with temperatures below 175 °C. Cold sintering of silica and its polymorphs to more than 90% relative density appears feasible, but phase transformations to quartz appear to be a feature of the densification process with a NaOH solution.

15. SUBJECT TERMS
Sciences of Extreme Materials, sintering, cold sintering, ceramic, silica, quartz, zinc oxide

16. SECURITY CLASSIFICATION OF:			17. LIMITATION OF ABSTRACT	18. NUMBER OF PAGES	19a. NAME OF RESPONSIBLE PERSON
a. REPORT	b. ABSTRACT	c. THIS PAGE			Victoria Blair/Michael Golt
Unclassified	Unclassified	Unclassified	UU	26	19b. TELEPHONE NUMBER (Include area code) (301) 802-6319/(410) 306-0946

Standard Form 298 (Rev. 8/98)
Prescribed by ANSI Std. Z39.18

Contents

List of Figures

List of Tables

1. Introduction

Cold sintering is a new technology first developed by researchers at Pennsylvania State University in 2016.[1] Unlike conventional sintering where mass transport and densification occur via thermally activated solid-state diffusion mechanisms, cold sintering operates by mass transport through or from a liquid medium. Experimentally, this is achieved by mixing ceramic powder with a liquid phase, typically adjusted in pH or containing a solution of ion compatible with the ceramic material and compressing it at several hundred megapascals pressure in a die heated to modest temperatures on the order of 100–300 °C. This process, which is noted to be similar to geological mechanisms of rock formation, enables consolidation of powders at significantly lower temperatures than conventional sintering. There are several potential benefits to cold sintering, including improvements in the efficiency and cost of sintering, co-consolidation of materials with differing properties such as ceramics and polymers, and the potential to sinter metastable phases, which would degrade at their sintering temperatures.

Literature reports on cold sintering initially focused on densification of hygroscopic materials such as sodium chloride (NaCl), barium titanate, and sodium nitrite mixed with aqueous mediums, demonstrating both densification and grain growth at low temperatures through application of heat and pressure.[2–4] Subsequent research efforts by multiple groups have investigated cold sintering of a far-wider range of soluble and insoluble materials, primarily focusing on electronic oxide ceramics. Though the exact mechanisms at work during cold sintering are highly material dependent and still under investigation and achieving pore-free "full" densities greater than 95% theoretical density has proven difficult, the technique has been demonstrated on over 100 materials.[5,6]

Specific examples of success with cold sintering include the sintering of zinc oxide (ZnO) using a NaCl liquid solution as a liquid phase. Conventional sintering of ZnO is conducted at temperatures above 1000 °C.[7] By using cold sintering, densification to more than 90% theoretical density was achieved by mixing with acetic acid solutions and sintering under 387 MPa pressure at 350 °C. Microstructural evaluation found that the grain size had increased from the starting powder size of approximately 100 nm to the micron scale, comparable to that which occurs at the much-higher temperature conventional sintering processes.[8] Cold sintering has also been demonstrated to enable processing of metastable materials such as tin(II) oxide, which degrades above 240 °C or zirconium tungstate, which degrades above 1100 °C, to greater than 90% theoretical density.[9]

A cold sintering setup was acquired by the US Army Combat Capabilities Development Command Army Research Laboratory for research into densification of metastable ceramics and glasses. Initial efforts investigated the cold sintering of ZnO, a well-characterized system, to ensure proper experimental operation and results comparable to literature reports. Subsequent studies focused on densification of silica (SiO_2), a system with amorphous and numerous crystalline phases (Fig. 1). Amorphous silica has been previously densified using cold sintering and the closely related technique of hydrothermal hot pressing. Ndayishimiye et al. densified SiO_2–polytetrafluoroethylene composites at polymer contents of up to 25% using 5-M NaOH and tetraethylorthosilicate (TEOS) mediums at temperatures of 270 °C and pressures of 430 MPa.[10] Taveri et al. were able to obtain more than 99% density using silica nanoparticles at room temperature in a 0.5-M NaOH solution at pressures of 600 MPa.[11] The phase transformation of amorphous SiO_2 to α-quartz was noted in experiments using the NaOH medium,[10,12] and aqueous mediums are known to destabilize the metastable cristobalite and stishovite phases of silica.[13] The primary objectives of these experiments were to identify critical process parameters for cold sintering of silica and determine if densification without phase transformation was possible.

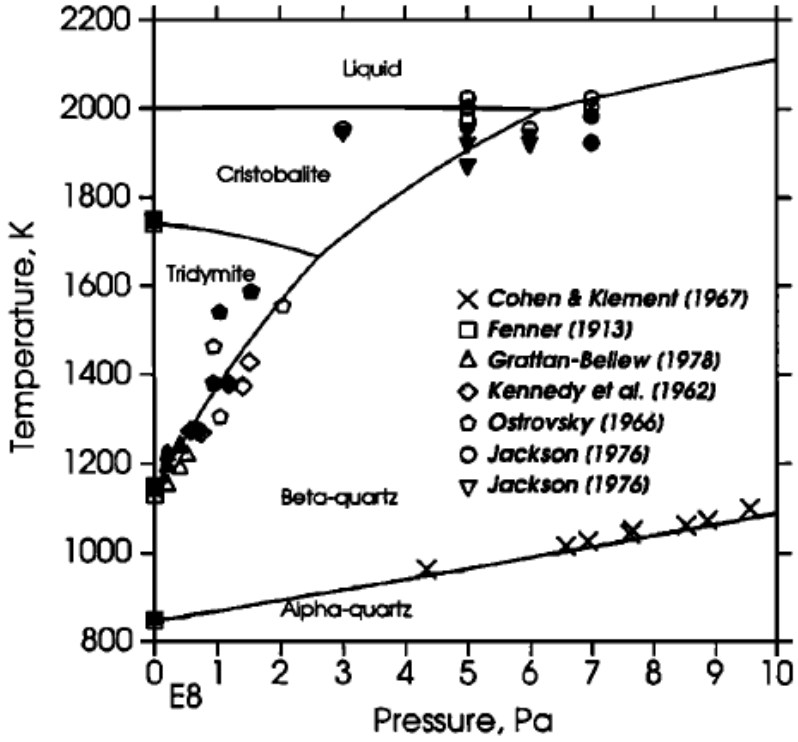

Fig. 1 Phase diagram of silica[14]

2. Experimental Methods

2.1 Powder Characterization

The particle size distribution and surface areas were characterized for all powders used in this study prior to experimentation. Particle size distribution was measured with a Horiba LA-960 laser diffraction particle size analyzer. Three separate measurements were taken on three samples from the powder reserve and averaged to obtain the D10, D50, and D90 characteristics and standard deviations. Powder surface area was measured using Brunauer–Emmett–Teller (BET) (Micromeritics TriStar II Plus) on a single sample of powder. Average measurements with standard deviations for all powders used in the study except ZnO, which proved too susceptible to agglomeration, are given in Table 1. Silica powders with similar particle size distributions were selected to minimize the well-understood impact of particle size on densification.

Table 1 Powder characterization data for materials used in the study

Powder	ZnO	NAM-4856 WG	US1133M-1	Cristobalite	5-Al:SiO_2	6-Ni:SiO_2
Supplier	US Research Nanomaterials, Inc	Nanostructured Materials	US Research Nanomaterials Inc	C.E.D, Process Minerals, Inc	Synthesized	Synthesized
Material	ZnO	SiO_2 (amorphous)	SiO_2 (quartz)	SiO_2 (cristobalite)	SiO_2 (amorphous, Al-doped)	SiO_2 (amorphous, Ni-doped)
Purity	>99%	99.99%	>99%	99.7%	N/A	N/A
D10 (µm)	N/A	1.088 ±0.003	1.09 ±0.01	0.83 ±0.08	0.40 ±0.13	0.47 ±0.09
D50 (µm)	20 nm[a]	1.48 ±0.01	1.50 ±0.06	1.7 ±0.1	1.0 ±0.2	1.1 ±0.1
D90 (µm)	N/A	2.34 ±0.02	2.4 ±0.1	3.1 ±0.3	3.4 ±0.2	2.24 ±0.05
Surface area (m^2/g)	65[a]	13	7.31	9.0	N/A	N/A

[a]Data for ZnO is reported by manufacturer.

Synthesis of Doped Silica Powders

Two powder lots of doped silica were synthesized by reaction of TEOS and water. Lot no. 5-Al:SiO_2 consisted of aluminum (Al)-doped silica and lot no. 6-Ni:SiO_2 was nickel (Ni)-doped silica. The synthesis method involved preparation of a 15-vol% solution of TEOS and ethanol in a closed beaker, which was sonicated for approximately 20 min in an ultrasonic bath. A second solution consisting of 25 mL of 1.0-M aqueous Ni or Al nitrate was prepared and allowed to stir on a hot plate in a fume hood. Upon dissolution of the nitrate, the solution was transferred to a buret. The TEOS solution was transferred to the stir plate and the nitrate was slowly added to the TEOS while stirring. The pH and temperature were monitored during

the process to ensure a slow reaction. Once the nitrate was exhausted, the hot plate was turned on and the ethanol was slowly evaporated using gentle heat and a nitrogen gas flush. The powder was dried in an oven overnight and crushed in a glass mortar and pestle.

2.2 Cold Sintering Apparatus

Feedstock material was prepared by mixing stock powders with solvent in measured quantities to achieve a targeted solids loading, typically 60 vol%. Mixing was performed in a FlackTek SpeedMixer in a closed 100-mL container. The speed profile was: 2000 rpm/30 s, 1400 rpm/20 s, 1600 rpm/10 s, and 2000 rpm/30 s. After mixing once, any large agglomerates were broken up manually and the mixing cycle was repeated. Mixed material was then immediately inserted into the die and cold sintered to minimize interaction with atmospheric humidity or evaporation.

Cold sintering was performed using an Across International 13-mm-diameter steel heated die set in an Instron 5984B load frame using a 150-kN load cell. Powder was placed in the die and pre-compacted at 74 MPa (10 ken). Temperature was monitored and controlled using a thermocouple inserted into the die wall. Pressure was controlled by operating the load frame under constant force mode using a 74 MPa/min (10 ken/min) ramp up to the desired load. The die temperature was recorded manually using the setpoint control thermocouple. Load and displacement were measured by the Bluehill software interface on the load frame and recorded as data files containing time, compressive load, and compressive displacement.

2.3 Specimen Analysis

After sintering, specimens were ejected from the die. Density was calculated by measuring the specimen mass and dimensions with a digital scale and vernier calipers. If the porosity was calculated to be under 10 vol% using this method, specimen density was measured using Archimedes' immersion. Specimens were imaged using scanning electron microscopy (SEM) on fracture surfaces and/or cross sections polished to 0.25-µm finish with diamond media. X-ray diffraction (XRD) scans of sintered specimens and raw powders were taken with a Bruker D2 Phaser to identify phase composition.

3. Results and Discussion

3.1 Cold Sintering of ZnO

ZnO was cold sintered using parameters based on research by Funahashi et al.[8] A nanopowder of ZnO (US Research Nanomaterials, 500 nm) was mixed with 5 wt% (22.6 vol%) of a 2-M acetic acid solution. Two specimens were cold pressed at 350 MPa, and a third at 500-MPa maximum load, with temperature ramped to 225 °C over approximately 20 min once maximum pressure was reached. Temperature and pressure were maintained for at least 1 h and then released. Four duplicate specimens were processed. Graphs of the load and displacement against time are shown in Fig. 2.

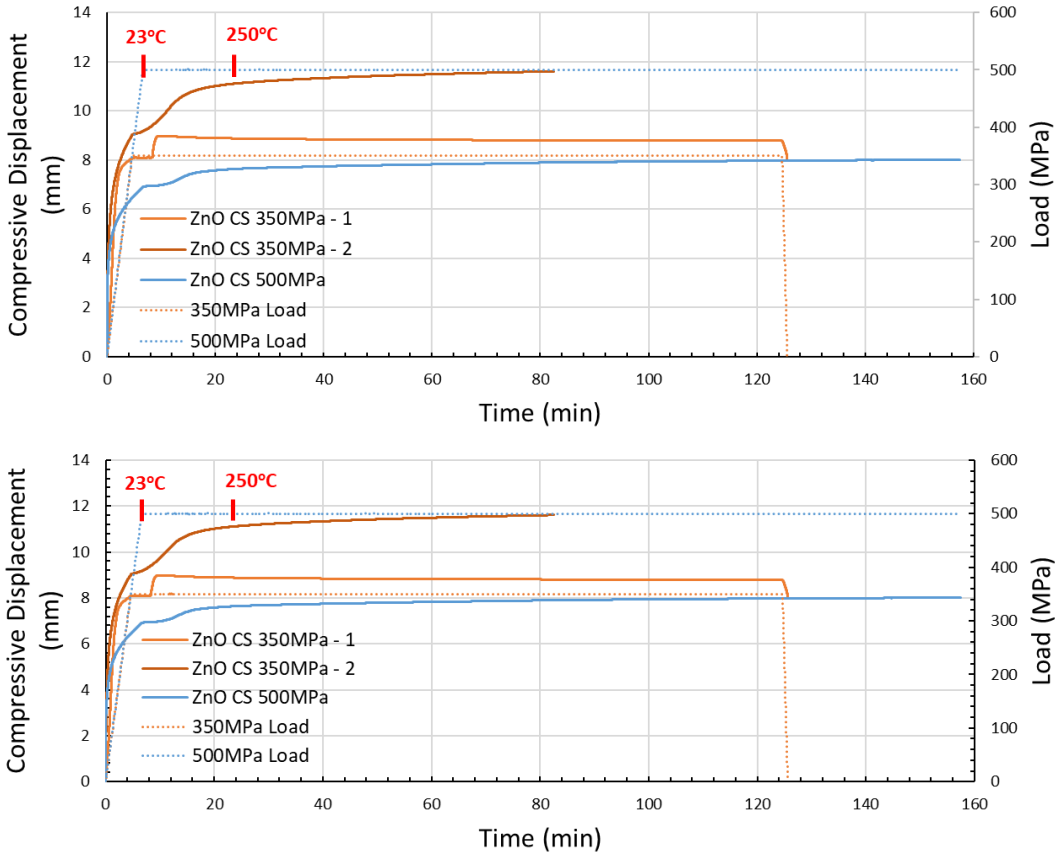

Fig. 2 Compressive load and compressive displacement plotted against time with temperature indicated for cold sintered ZnO specimens

The curves show a nonlinear increase in displacement with applied load up to the maximum, indicative of a combined elastic response as well as likely particle rearrangement from the compaction process. In all cases, the displacement reached a brief steady state after the load reached maximum and then increased as

temperature was applied. This increase is indicative of thermally activated densification occurring, and except for curve ZnO CS 350 MPa - 1 (see Fig. 2) continues to occur at an exponentially slowing rate for the duration of the experiment.

The final densities of the specimens measured by mass and calipers are recorded in Table 2. The specimen cold sintered at 500 MPa reached a relative density of 91.5%, significantly greater than that which can be obtained by particle compaction and rearrangement. SEM evaluations of cross-sectioned parts (Fig. 3) revealed significant cracking and irregular densification within the specimen, but also grain coarsening and high density on the micron scale consistent with the low porosities measured. The inconsistent densification and spalling could indicate possible inhomogeneity in the distribution of liquid phase either postmixing or during the cold sintering process. Overall, these results are consistent with those observed by Funahashi et al.,[8] demonstrating that the cold sintering apparatus is operating as expected.

Table 2 Densities and calculated porosities measured via geometric methods for cold sintered ZnO. Data for specimen 1AR223 is an estimate only due to the specimen spalling into irregular geometries during die removal.

Specimen	Load	Density	Porosity
1AR206	350 MPa	4.76 g/cm^3	15.2%
1AR223	350 MPa	>5 g/cm^3	<10%
1AR227	500 MPa	5.13 g/cm^3	8.5%

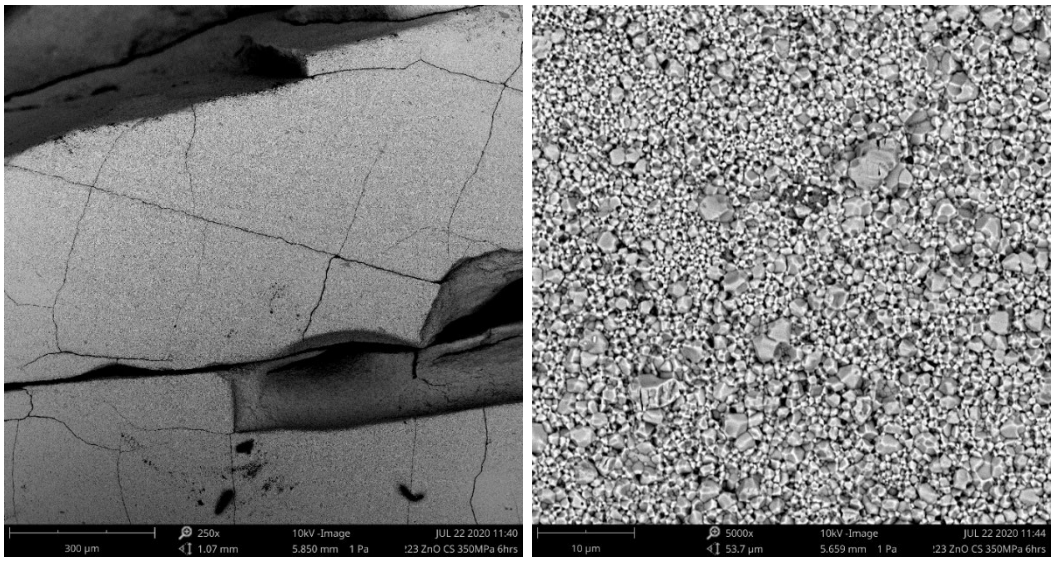

(a) (b)

Fig. 3 SEM images of cross-sectioned and polished ZnO specimen 1AR223 at a) 250× and b) 5000× magnification

3.2 Cold Sintering of SiO_2

3.2.1 Initial SiO_2 Experiments

The initial investigation of the cold sintering of SiO_2 was performed using amorphous silica powder (NAM 4856-WG) in a 5-M NaOH solution at liquid loadings of 12 wt% (24 vol%) to 25 wt% (43 vol%). Cold sintering was performed at a temperature of 250 °C with a pressure of 500 MPa and hold times from 1.5 to 24 h. Specimen details and measured densities are presented in Table 3 with load-displacement curves in Fig. 4.

Table 3 Solids loadings, hold times, measured sintered density, and calculated porosities for initial SiO_2 specimens cold sintered in a 5-M NaOH solution at 250 °C/500 MPa

Specimen	Liquid loading	Hold time	Density	Porosity
1AR228	12 wt% (24 vol%)	1.5 h	1.84 g/cm^3	30.6%
1AR232	16 wt% (30 vol%)	6 h	2.39 g/cm^3	9.2%
1AR233	24 wt% (42 vol%)	6 h	2.47 g/cm^3	6.4%
1AR238	25 wt% (43 vol%)	24 h	2.52 g/cm^3	5.1%

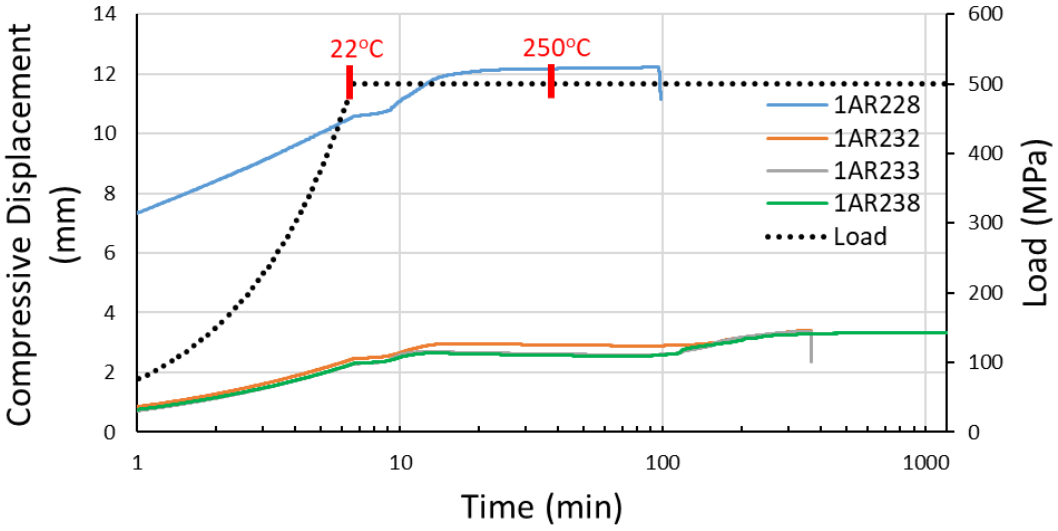

Fig. 4 Compressive displacement and load plotted against time (log scale) for initial SiO_2 specimens in Table 3. The initiation of heating and time at which maximum temperature was reached are indicated on the load curve.

Specimen 1AR228 was sintered with a liquid loading of 12 wt% (24 vol%). As the die was heated to 250 °C it exhibited a surge of compressive displacement, followed by an exponentially decaying increase in displacement during the hold at 250 °C, indicating that some consolidation mechanisms were activated by the increase in temperature and remained at work during the hold. However, it had a final sintered density of only 69.4%, which is comparable to the theoretical packing limit of

approximately 65%, suggesting that most of the displacement was due to mechanical particle rearrangement instead of densification mechanisms. This specimen also exhibited an unusually large compressive displacement relative to the other specimens, which is attributed to operator error forgetting to apply the 10-kN pre-compaction in this specimen.

All specimens with a NaOH concentration above 12 wt% (24 vol%) exhibited the initial surge of displacement seen in specimen 1AR228 as they were heated, but also exhibited a second sudden surge of displacement about 1.5 h into the cold sintering process. The density of these specimens was greater than 90% theoretical, with density increasing with increased liquid loading and hold time. A maximum density of 94.9% was obtained in specimen 1AR238, which was cold sintered with 25 wt% (43 vol%) of the NaOH solution for 24 h. SEM analysis of polished cross sections (Fig. 5) confirmed that the material had densified to the point that closed porosity had formed, with only small pores present. XRD scans of sintered pellets (Fig. 6) found that the previously amorphous silica had converted to quartz during the process.

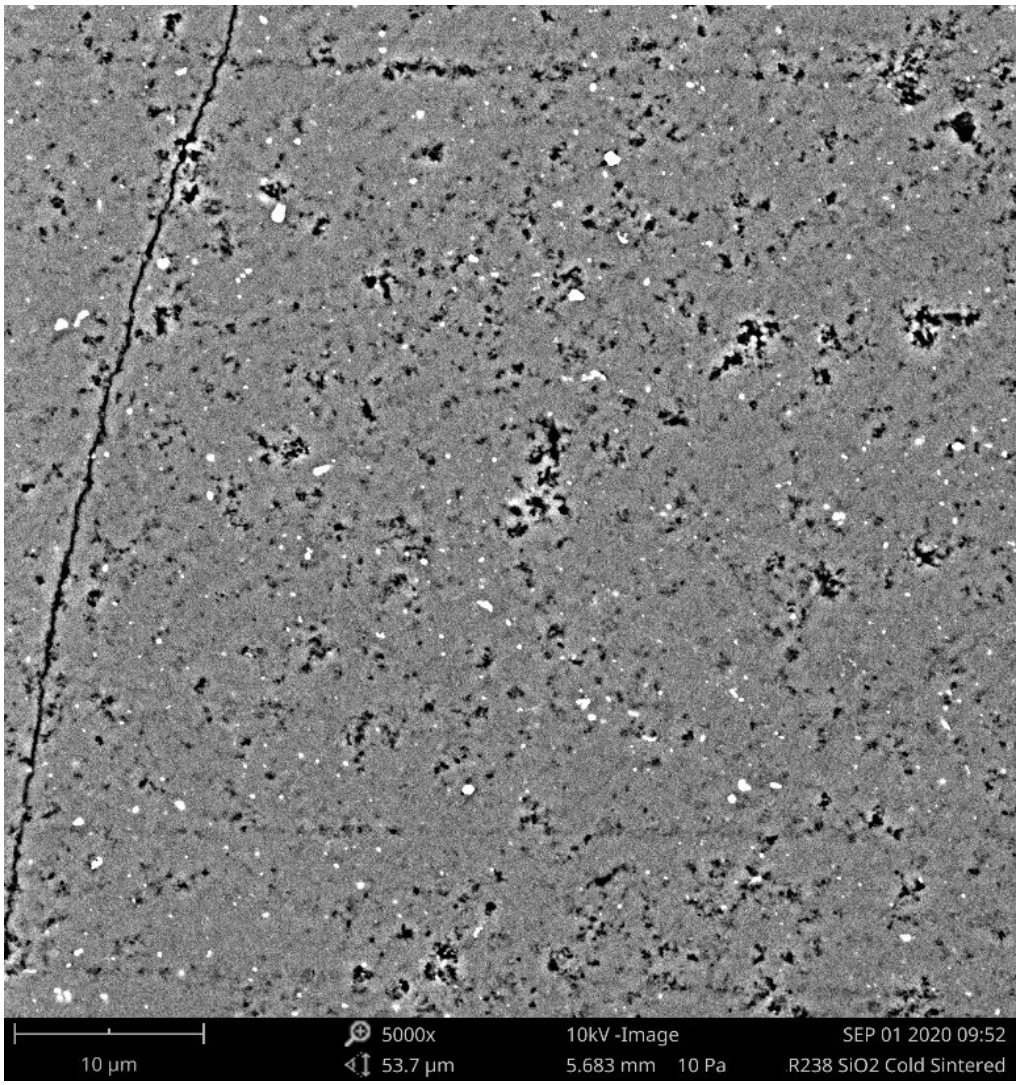

Fig. 5 SEM image of specimen 1AR238 (SiO_2, cold sintered at 250 °C/500 MPa for 24 h) polished and cross-sectioned showing small-scale residual porosity

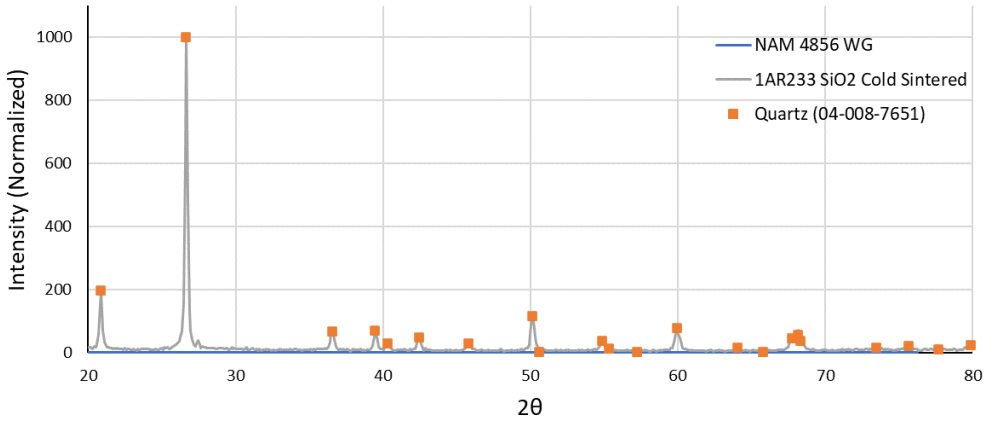

Fig. 6 XRD scan of cold sintered specimen 1AR233 demonstrating conversion of amorphous SiO_2 powder (not visible via XRD) into quartz

The relatively large time delay between the application of pressure and densification is a curious and unique feature to the cold sintering of SiO_2 that was also observed by Ndayishimiye et al.[10] In their transmission electron microscopy studies, they noted the nucleation and growth of quartz nanoparticles during cold sintering, which when under pressure could be a mechanism promoting densification like those active in reaction sintering. There is an apparent correlation between the phase transformation and densification; specimen 1AR288, which was cold sintered with a lower liquid content and did not densify, remained amorphous, while all specimens that did densify transformed to quartz. This indicates the phase transformation to quartz is intimately linked with the densification process in cold sintering and likely occurs during the precipitation and grain growth process.

3.2.2 SiO_2 Design of Experiments

Following the initial results, a design of experiments (DOE) style set of runs were performed to assess the relative impact of process parameters on densification. Liquid loading was set at 37.5 vol%, soak time at 4 h, and temperature at 250 °C, while the NaOH concentration, applied load, powder type, and timing of the temperature ramp relative to the pressure ramp all varied per Table 4 over eight experimental runs in a $2^{(4-1)}$ factor DOE. Load-displacement curves (Fig. 7) as well as final density (Table 4) of the pellets were collected, with density as a percentage used as the primary response.

Table 4 DOE variable parameters and sintered density and porosity

Specimen	NaOH concentration	Heating timing	Applied pressure	Powder type	Sintered density	Sintered porosity
1AR241	1 M	Before pressure	150 MPa	Quartz	1.43 g/cm^3	45.0%
1AR262	10 M	Before pressure	150 MPa	Amorphous	1.74 g/cm^3	34.3%
1AR244	1 M	After pressure	150 MPa	Amorphous	1.35 g/cm^3	48.9%
1AR250	10 M	After pressure	150 MPa	Quartz	1.84 g/cm^3	30.0%
1AR251	1 M	Before pressure	650 MPa	Amorphous	1.03 g/cm^3	60.0%
1AR253	10 M	Before pressure	650 MPa	Quartz	1.60 g/cm^3	40.0%
1AR255	1 M	After pressure	650 MPa	Quartz	2.07 g/cm^3	22.0%
1AR260	10 M	After pressure	650 MPa	Amorphous	2.34 g/cm^3	12.0%

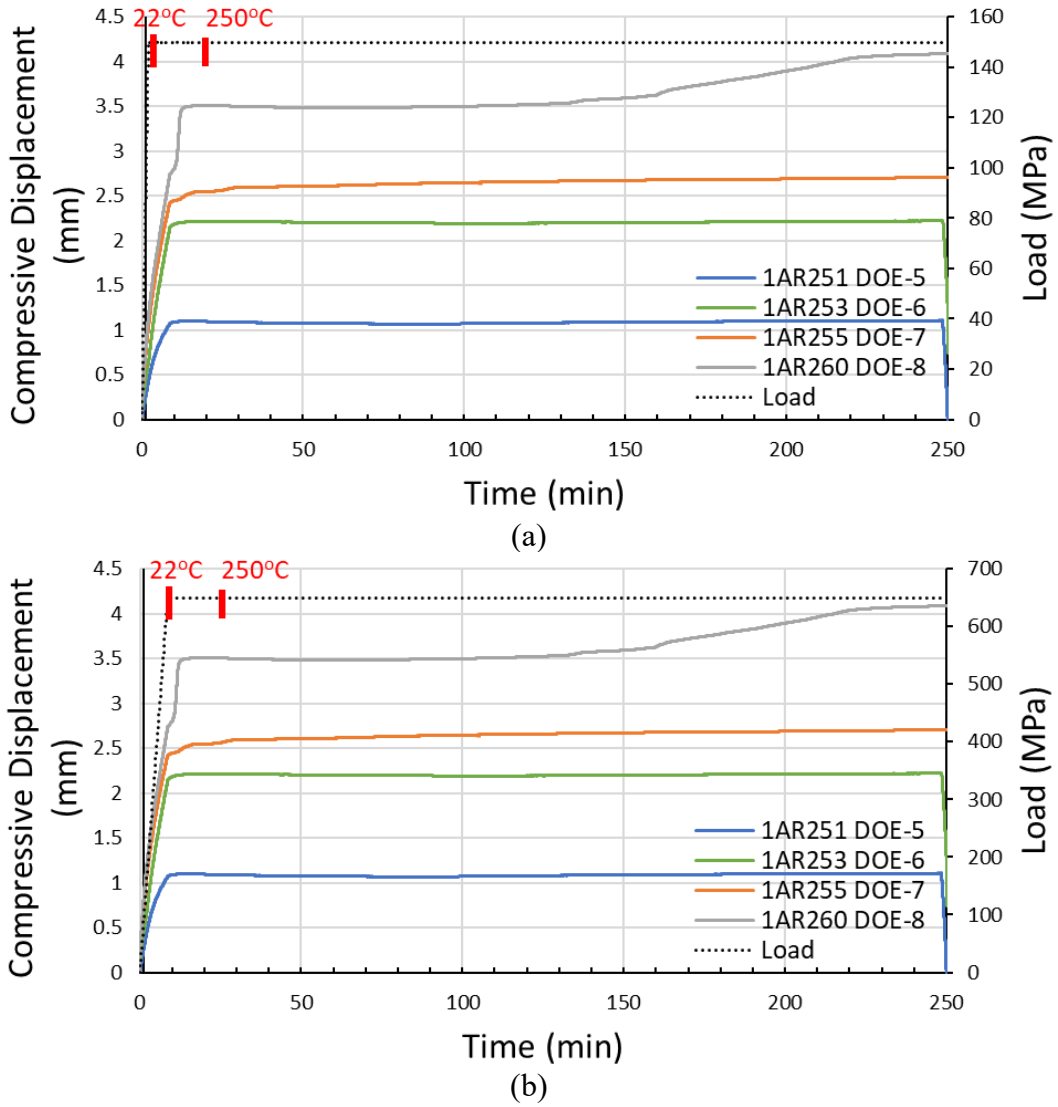

Fig. 7 Load-displacement curves for the DOE specimens separated into a) all specimens with a 150-MPa load and b) all specimens with a 650-MPa load

Pareto analysis (Fig. 8) of the results found that the variables with the strongest influence on final density were the NaOH concentration, timing of the heating, and two-way interactions between either NaOH concentration and powder type or heating timing and pressure. Mean relative density increased from 56% at specimens sintered with the 1-M NaOH concentration to 71% at specimens sintered with 10-M concentration, which is consistent with a chemically activated dissolution/precipitation mechanism proposed for cold sintering. Likewise, when the specimen was heated to 250 °C prior to application of pressure, mean relative density was only 55%, increasing to 72% in specimens where pressure was applied prior to heating. Despite being confined within the steel die, the vaporization of the liquid medium appeared to have ejected sufficient moisture from the specimens to

prevent cold sintering, which was apparently prevented during runs where pressure was increased first, potentially due to the decrease in porosity from mechanical particle rearrangement and densification as the part was heating, entrapping more moisture within the part.

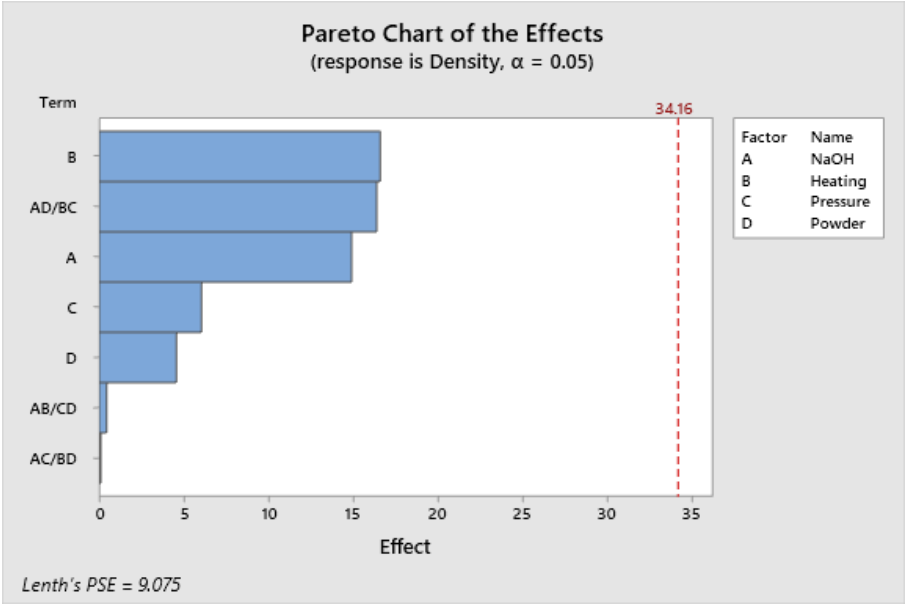

(a)

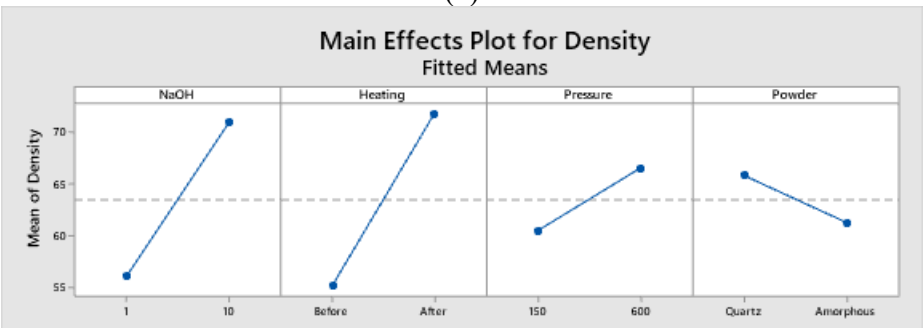

(b)

Fig. 8 a) Pareto chart of effects alongside b) main effects plot for density

Analysis of the two-way interactions (Fig. 9) is confused by the confounding of the NaOH/powder-type interactions with the heating/pressure interactions. Potential contributions could be a lower interactivity between quartz and the NaOH solution, or a dependence on high pressure to achieve maximum particle rearrangement to prevent moisture loss during heating. As the densification involves a phase transformation to quartz, it is most likely that the quartz powder is less sinterable than amorphous, but a direct comparison of quartz to amorphous SiO_2 is required to establish this.

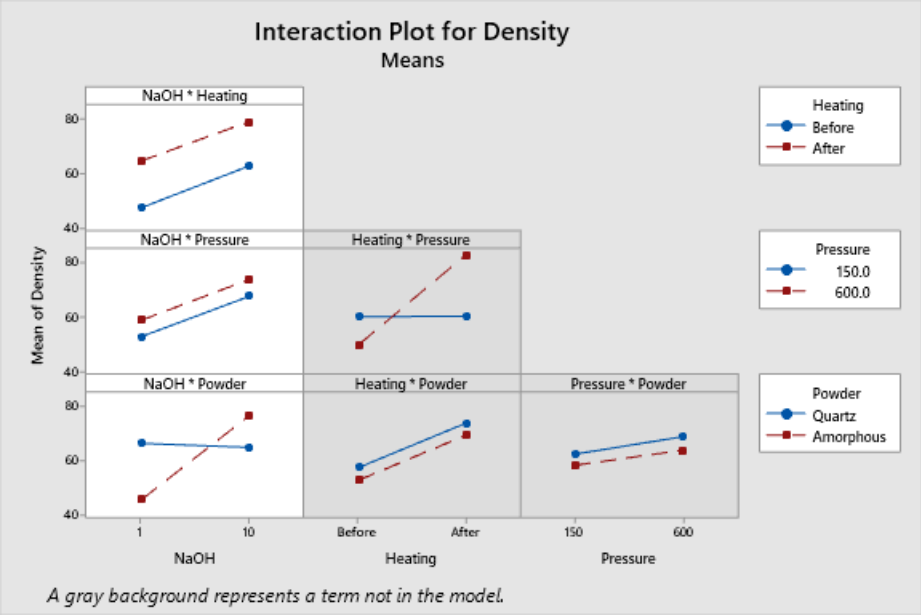

Fig. 9 Interaction plot of mean density showing main effects and interactions

3.2.3 Phase Experiments

A final set of experiments was performed to further investigate the effects of phase and metal-ion doping on the cold sintering behavior of SiO_2. A set of three cold sintering runs using amorphous SiO_2 (NAM 4856-WG) in 20 wt% of 5-M NaOH solution at a temperature of 250 °C at 500-MPa load for 4 h was performed to establish and characterize baseline results and variability. Runs were then performed under the same conditions using amorphous powder doped with Ni (6-Ni:SiO_2)and Al (5-Ni:SiO_2) ions, cristobalite powder (C.E.D. Process Minerals, Inc), and quartz powder (USNM 1133-W). Their final density and load-displacement behavior were then compared to the amorphous SiO_2 baseline to identify the effect the different powders had on cold sintering (Table 5 and Fig. 10).

Table 5 Specimen information and sintered densities for doping and phase experiments

Specimen	Phase	Temperature	Sintered density	Sintered porosity	Sintered phase
1AR233	Amorphous	250 °C	2.47 g/cm^3	6.6%	Quartz
1AR304	Amorphous	250 °C	2.48 g/cm^3	6.3%	Quartz
1AR293	Amorphous	250 °C	2.36 g/cm^3	11.1%	Quartz
1AR298	Al-doped	250 °C	2.47 g/cm^3	6.7%	Quartz
1AR299	Ni-doped	250 °C	2.15 g/cm^3	18.9%	Quartz
2AR118	Cristobalite	250 °C	2.37 g/cm^3	10.7%	Quartz
2AR119	Cristobalite	250 °C	2.27 g/cm^3	14.2%	Quartz
2AR123	Cristobalite	175 °C	2.08 g/cm^3	21.7%	Cristobalite
2AR120	Cristobalite	100 °C	1.99 g/cm^3	24.8%	Cristobalite
3AR001	Quartz	250 °C	2.14 g/cm^3	19.1%	Quartz

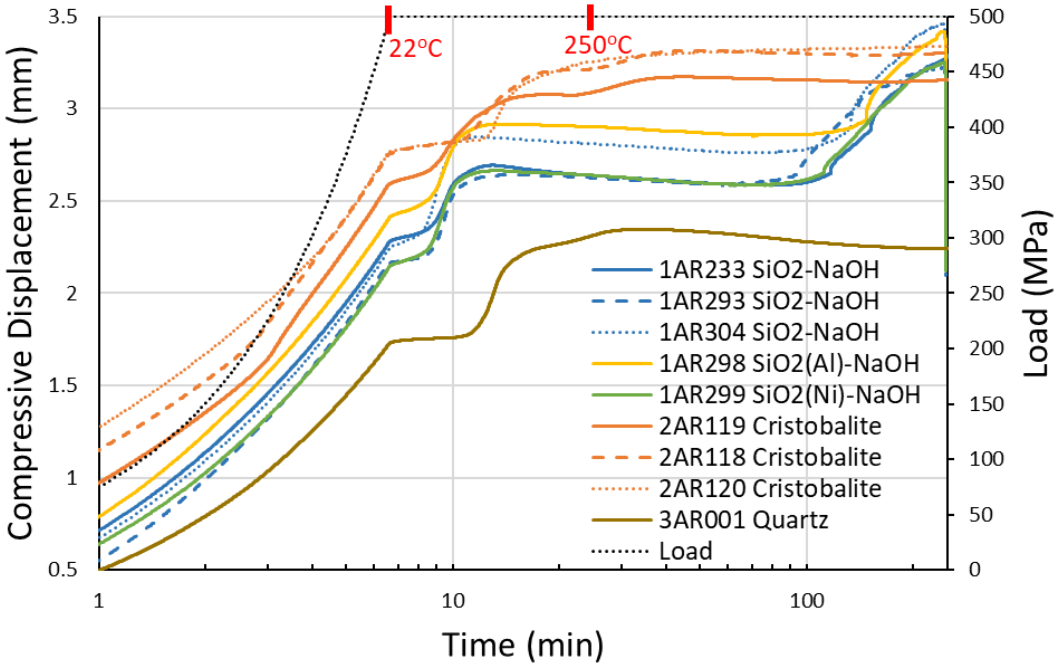

Fig. 10 Compressive load and displacement plotted against time with temperature indicated for specimens in Table 5

The three amorphous SiO_2 specimens (1AR233, 1AR304, and 1AR293) all exhibited similar load displacement behavior with increases in displacement during heating and at approximately 1.5 h into the hold (Fig. 10). Their porosities were 6.6%, 6.3%, and 11.1%, giving a mean porosity of 8.0% and standard deviation of 2.7%. The Al- and Ni-doped powders exhibited similar load-displacement curves to the amorphous baseline. The porosity of the Al-doped specimen was comparable to the amorphous specimens at 6.7%, but the porosity of the Ni-doped specimen was 18.9%, indicating that it densified substantially less than the amorphous

material (p-value of 0.02). Based on these results, metal-ion doping of silica with Al or Ni does not appear to enhance densification during cold sintering.

Cold sintering with quartz resulted in a high porosity of 19.1%, with the load-displacement curve not exhibiting any increase in displacement after heating. This clarifies that the interaction observed in the DOE is related to phase content; reexamining the data in Fig. 9 in light of this new data demonstrates that, under low-densification conditions, phase does not significantly impact final porosity, but under conditions where amorphous silica will densify, quartz powder is less sinterable.

The cristobalite specimens exhibited a greater increase in displacement during and immediately after heating than the baseline amorphous specimens and did not have an increase in displacement at extended hold times. While the mean porosity of the cristobalite specimens was higher than the amorphous specimens (12.5% vs. 8.0 ±2.7%), it was not outside the 95% confidence limit of variation. The cristobalite specimens were found to have phase transformed to quartz, similar to the amorphous silica specimens (Fig. 11). It appears that, unlike in amorphous silica, the phase transformation to quartz from cristobalite occurs immediately upon heating, which is consistent with the lower phase stability of cristobalite. Two additional cristobalite specimens were cold sintered at 175 and 100 °C to investigate whether densification could be achieved without the phase transformation. Both retained significant cristobalite, but also had more than 20% porosity.

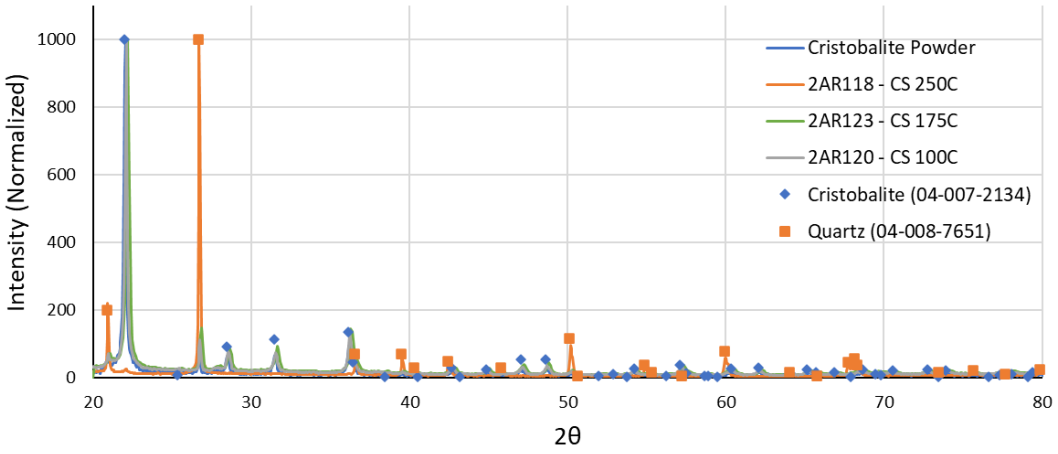

Fig. 11 XRD spectra for cristobalite powder and specimens cold sintered at 250, 175, and 100 °C

Based on these results, doping SiO_2 powders does not appear to increase densification, and in the case of Ni is actively detrimental to densification. Cristobalite sinters to final densities comparable to amorphous silica, but with the

phase-transformation couple surge in densification occurring immediately upon heating instead of after a half-hour delay. Quartz does not densify significantly. Attempts to retain densification while avoiding the phase transformation by reducing the sintering temperature proved unsuccessful. It can be concluded therefore that the phase transformation to quartz is not just a byproduct of SiO_2 precipitating in its most stable phase during sintering, but that it actively drives densification mechanisms.

4. Conclusions

Cold sintering was used to successfully densify ZnO and SiO_2. ZnO was sintered to a maximum relative density of 91.5% using processes based on literature reports, verifying the proper operation of the apparatus. SiO_2 was found to be sinterable to more than 95% theoretical using a NaOH solution at a concentration more than 5 M and liquid content of 37.5 vol%. The load-displacement behavior exhibited an unusual incubation time of about 1.5 h before densification occurred. The influence of NaOH concentration, applied load, timing of the temperature ramp, and phase of SiO_2 on densification were investigated, and NaOH concentration and timing of the temperature ramp were found to have the strongest influence on densification. In general, densification was optimized by using a high-molarity NaOH solution and high applied load, with load applied before temperature. The cold sintering behavior of SiO_2 doped with Al and Ni as well as quartz and cristobalite phase SiO_2 was compared to nominally pure amorphous phase SiO_2. The dopants were found to hinder densification, while the phase transformation to quartz was observed to be a critical part of the densification process during sintering. Overall, cold sintering proved capable of densifying multiple phases of SiO_2 to more than 90% theoretical density at temperatures of 250 °C, significantly below conventional processing temperatures.

5. References

1. Guo J, Guo H, Baker AL, Lanagan MT, Kupp ER, Messing GL, Randall CA. Cold sintering: a paradigm shift for processing and integration of ceramics. Angew Chem Int Ed. 2016;55(38):11457–61.

2. Guo J, Berbano SS, Guo H, Baker AL, Lanagan MT, Randall CA. Cold sintering process of composites: bridging the processing temperature gap of ceramic and polymer materials. Adv Funct Mater. 2016;26(39):7115–21.

3. Guo H, Guo J, Baker A, Randall CA. Hydrothermal-assisted cold sintering process: a new guidance for low-temperature ceramic sintering. ACS Appl Mater Interfaces. 2016;8(32):20909–15.

4. Guo H, Baker A, Guo J, Randall CA. Cold sintering process: a novel technique for low-temperature ceramic processing of ferroelectrics. J Am Ceram Soc. 2016;99(11):3489–507.

5. Guo J, Floyd R, Lowum S, Mari, J-P, Beauvoir THd, Seo J-H, Randall CA. Cold sintering: progress, challenges, and future opportunities. Annu Rev Mater Res. 2019;49(1):275–95.

6. Vakifahmetoglu C, Karacasulu L. Cold sintering of ceramics and glasses: a review. Curr Opin Solid State Mater Sci. 2020;100807.

7. Hynes AP, Doremus RH, Siegel RW. Sintering and characterization of nanophase zinc oxide. J Am Ceram Soc. 2002;85(8):1979–87.

8. Funahashi S, Guo J, Guo H, Wang K, Baker AL, Shiratsuyu K, Randall CA. Demonstration of the cold sintering process study for the densification and grain growth of ZnO ceramics. J Am Ceram Soc. 2017;100(2):546–53.

9. Galotta A, Sglavo VM. The cold sintering process: a review on processing features, densification mechanisms and perspectives. J Eur Ceram Soc. 2021;41(16):1–17.

10. Ndayishimiye A, Tsuji K, Wang K, Bang SH, Randall CA. Sintering mechanisms and dielectric properties of cold sintered (1-x) SiO_2 - x PTFE composites. J Eur Ceram Soc. 2019;39(15):4743–51.

11. Taveri G, Grasso S, Gucci F, Toušek J, Dlouhy I. Bio-inspired hydro-pressure consolidation of silica. Adv Funct Mater. 2018;28(48):1805794.

12. Ndayishimiye A, Largeteau A, Mornet S, Duttine M, Dourges M-A, Denux D, Verdier M, Gouné M, Hérisson de Beauvoir T, Elissalde C, et al. Hydrothermal sintering for densification of silica. Evidence for the role of water. J Eur Ceram Soc. 2018;38(4):1860–70.

13. Linn NMK, Mandal M, Li B, Fei Y, Landskron K. Insights into the hydrothermal metastability of stishovite and coesite. ACS Omega. 2018;3(10):14225–28.

14. Swamy V, Saxena SK, Sundman B, Zhang J. A thermodynamic assessment of silica phase diagram. J Geophys Res Solid Earth. 1994;99(B6):11787–94.

List of Symbols, Abbreviations, and Acronyms

Al	aluminum
ARL	Army Research Laboratory
BET	Brunauer–Emmett–Teller (method to determine surface area)
DEVCOM	US Army Combat Capabilities Development Command
DOE	design of experiments
N/A	not applicable
NaCl	sodium chloride
NaOH	sodium hydroxide
Ni	nickel
rpm	revolutions per minute
SEM	scanning electron microscopy
SiO_2	silica
TEOS	tetraethylorthosilicate
XRD	X-ray diffraction
ZnO	zinc oxide

1 (PDF) DEFENSE TECHNICAL INFORMATION CTR DTIC OCA

1 (PDF) DEVCOM ARL FCDD RLD DCI TECH LIB

3 (PDF) DEVCOM ARL FCDD RLW ME V BLAIR M GOLT FCDD RLW WB L HLUBB